

Modification of Calcium Oxide from Green Mussel Shell with Iron Oxide as a Potential Adsorbent for the Removal of Iron and Manganese Ions from Acid Mine Drainage

Widia Purwaningrum^{1,2}, Hasanudin Hasanudin², Addy Rachmat², Fahma Riyanti^{1,2}, Poedji Loekitowati Hariani^{2*}

¹ Doctoral Program of Mathematics and Natural Sciences, Faculty of Mathematics and Natural Sciences, Sriwijaya University, Jalan Padang Selasa No 524 Bukit Besar, Palembang 30139, South Sumatra, Indonesia

² Department of Chemistry, Faculty of Mathematics and Natural Sciences, Sriwijaya University, Jalan Palembang-Prabumulih Km 32, Indralaya, Ogan Ilir, Indonesia

* Corresponding author's email: puji_lukitowati@mipa.unsri.ac.id

ABSTRACT

Acid mine drainage (AMD) has the characteristics of high heavy metal ion content and low pH. This study aimed to synthesize the CaO/Fe₃O₄ composite for the adsorption of iron and manganese ions from acid mine drainage. CaO was synthesized from the shells of green mussels (*Perna viridis*). The CaO/Fe₃O₄ composites were characterized using XRD, BET surface area, SEM-EDS, and VSM. The functional groups of the composite before and after adsorption were analyzed using FTIR. The adsorption of Fe(II), Fe(III), and Mn(II) ions was carried out with the batch method to determine the effect of pH, contact time, and initial concentration of metal ions. The CaO/Fe₃O₄ composite has magnetic properties, as indicated by the saturation magnetization value of 65.49 emu/g. The Langmuir and Freundlich isotherm models were used to describe the adsorption isotherm of the composite for Fe(II), Fe(III), and Mn(II) ions. Investigations were also conducted on adsorption kinetics, including pseudo-first-order and pseudo-second-order, as well as adsorption thermodynamics comprising free energy, enthalpy, and entropy. Pseudo-first-order and Langmuir isotherms are suitable to describe the adsorption of Fe(II), Fe(III), and Mn(II) ions with adsorption capacities of Fe(III) > Fe(II) > Mn(II). Moreover, the adsorption of all ions using the composite occurred spontaneously. The removal effectiveness for Fe and Mn ions from AMD using CaO/Fe₃O₄ composite, reached 90.41 and 97.59%, respectively, in volume 100 mL AMD, composite mass 0.4 g, and a contact time of 60 minutes.

Keywords: CaO/Fe₃O₄, green mussel shell, adsorption, iron, manganese, acid mine drainage.

INTRODUCTION

Mineral resources play an important role in sustainable community development. In the long term, attention must be paid to environmental aspects such as acid mine drainage. During the mining process, heavy metals are released, which leave residues in open areas. AMD is formed due to the oxidation of sulfide minerals produced from high sulfate concentrations, hydronium, and metals [Candeis et al., 2014; Carrilo-Gonzales et al., 2022]. In the mining process, this condition pollutes resources, including ground and surface water, as well as endangers the ecological

environment, specifically around the mining area. Furthermore, AMD causes the loss of biodiversity and aquatic ecosystems [Kefeni et al., 2017]. The characteristics of AMD, such as low pH, high of salinity, suspended solids, and concentrations of heavy metals [Tong et al., 2022; Li et al., 2022]. Previous studies stated that AMD contains heavy metals, such as Fe, Mn, Zn, Pb, Hg, Al, Cu, and Cd [Westholm et al., 2014; Nunez-gomez et al., 2019]. Hence, efforts are needed to overcome the negative impacts.

In general, there are two methods used for AMD processing, namely active and passive treatment [Johnson and Hallberg, 2005]. Active

treatment is used in mines that are still operating, while passive treatment is used for closed and abandoned mines [Trumm, 2010]. The active treatment method is more suitable for the mines that are still in operation, due to the limited space for the remediation system, as well as large and fluctuating flow rates during mining. It needs to be handled quickly and effectively. Several methods have been reported to reduce the negative impact of AMD, including coagulation [Choi et al., 2000], electrochemical [Chartrand et al., 2003], reverse osmosis [Zhong et al., 2007], filtration [Trumm, 2010], neutralization [Pereira et al., 2020], and adsorption [Raiman et al., 2021].

Adsorption is one of the effective methods for removing metal ions from the solution [Markovic et al., 2020]. The active treatment has the advantages of low cost, flexibility, simple design, and easy operation [Ahmaruzzaman, 2011; Markovic et al., 2020]. Some adsorbents such as lignite [Mohan and Chander, 2006], zeolite [Motsi et al., 2011], bone char [Sicupira et al., 2015], activated carbon [Aprianti et al., 2017], carbon nanotube [Rodriguez and Leiva, 2020], organic biomixture [Raiman et al., 2021], and, waste pyrolysis ash [Li et al., 2022], showed promising results to reduce heavy metal ions from AMD.

CaO is an oxide that is widely applied as a catalyst and adsorbent of toxic compounds [Thakur et al., 201]. As an adsorbent, it has advantages, such as large surface area, low cost, safe for humans, fast kinetics, and effective for removing heavy metal ions from water. In addition, it has been used to adsorb dyes from the textile, pharmaceutical, and agricultural waste industries, as well as to absorb the CO₂ gas [Thakur et al., 2021; Granados-Pichardo et al., 2020]. The combination of adsorption using CaO and electrochemical methods effectively increased pH and reduced heavy metal ions, such as Fe, Mn, Co, Ni Cu, and Zn from AMD [Orescanin and Kollar, 2012]. The alkaline nature of CaO can increase the pH of AMD, which is acidic.

Naturally, CaO is obtained from several materials containing CaCO₃, such as eggshells [Kasirajan et al., 2022], mollusk shells [Thakur et al., 2021], and limestone [Sisca et al., 2021]. Green mussel is one of the shellfish consumed by Indonesians. The shell is solid waste that is generally dumped and left in landfills, but it is a potential source of CaO as an adsorbent. The advantages include locally available, abundant, and low cost sources. Mollusk shells contain 95–99.9% calcium

carbonate and 0.1–5% organic material [Marxen et al., 2003; White et al., 2007]. Several adsorbent had been modified with ferrite compounds and shows high adsorption capacity, specific surface area, easy separation, physical flexibility, and chemical stability [Foroutan et al., 2020; Liu et al., 2019]. Among ferrite compounds, magnetite (Fe₃O₄) has a special feature namely superparamagnetic properties. In addition, Fe₃O₄ is biocompatible, biodegradable, non-toxic to humans and has been used in several studies to remove heavy metals [Yew et al., 2020].

This study aimed to synthesize the CaO/Fe₃O₄ composite, used for the adsorption of Fe(II), Fe(III), and Mn(II) ions from the solution. CaO was synthesized from green mussel shells, while the adsorption test includes the performance of solution pH, contact time, and initial concentration. The isotherms, kinetics, and thermodynamics of adsorption were also investigated. Furthermore, the CaO/Fe₃O₄ composite was applied to removal of Fe, and Mn ions as well as to increase the pH of the AMD solution.

MATERIALS AND METHOD

Materials

The materials used include Green mussel shell, Iron(III) chloride hexahydrate (FeCl₃·6H₂O), Iron(II) chloride tetrahydrate (FeCl₂·4H₂O), Sodium hydroxide (NaOH), Hydrochloric acid (HCl), Iron(II) standard solution 1000 ppm, Iron (III) standard solution 1000 ppm, and manganese(II) standard solution 1000 ppm from Merck, Germany. Meanwhile, AMD was taken from a coal mine, in Tanjung Enim, South Sumatra, Indonesia.

CaO/Fe₃O₄ composite preparation

Green mussel shells were cleaned of impurities and washed with aquadest, they were then heated in the oven for 10 hours at a temperature of 105°C. After drying, they were milled, to obtain a size of 200 mesh. The shell powder was calcined at a temperature of 800°C for 8 hours, while the CaO powder was stored in airtight plastic.

The CaO/Fe₃O₄ composite was made with a mass ratio of CaO:Fe₃O₄=2:1. FeCl₃·6H₂O ions (2.33 g), FeCl₂·4H₂O (0.859 g) were dissolved into 25 mL deionized water, the mixture was stirred using a magnetic stirrer at 200 rpm with N₂

gas flowed for 30 minutes. About 2 g of CaO was added to the mixture, then heated on a hotplate at a temperature of 60°C and followed by stirring. Subsequently, 1 M of NaOH solution was added to the mixture gradually until a pH of ± 10 was obtained, and a black precipitate was formed. The composite obtained was washed with deionized water until it became neutral, followed by drying in an oven for 3 hours at a temperature of 105°C, and then used as an adsorbent.

Material characterization

The crystal structure and size were determined using X-ray Diffraction (XRD PANalytical) with incident radiation of Cu K α (1.54) and range $2\theta = 10\text{--}90^\circ$, while the surface area was determined with the Brunauer-Emmet-Teller (BET) method (Quadrasorb station I type I 7.01) using nitrogen gas adsorption-desorption. The morphology and elemental composition were analyzed with Scanning Electron Microscope-Energy Dispersive Spectrometer (SEM-EDS JEOL JSM 6510 LA), while the saturation magnetization was measured using a Vibrating Sample Magnetometer (VSM Oxford Type 1.2 T). The functional groups were analyzed using the Fourier Transform Infra-Red (FTIR Prestige 21 Shimadzu) at a wave number of 400–4000 cm^{-1} . The concentration of metal ions was determined using Atomic Absorption Spectroscopy (Shimadzu AA 7000).

Adsorption

The adsorption process was carried out with the bath method, the variables include the pH of the solution, the contact time, and the initial concentration of the dye. About 0.1 g of the CaO/Fe₃O₄ composite was added into 100 mL solution of Fe(II), Fe(III), and Mn(II) with a concentration of 10 mg/L. The pH of the mixture was adjusted in the range of 2–9 using a solution of 0.1 M HCl and NaOH. The mixture was stirred at 120 rpm and room temperature for 30 minutes. Furthermore, the concentrations of Fe(II), Fe(III), and Mn(II) ions were measured using AAS. The effect of contact time was assessed in the range of 0–120 minutes, while the initial metal ions concentrations were in the range of 5–60 mg/L.

The adsorption isotherm was determined with a composite mass of 0.1 g, Fe(II), Fe(III), and Mn(II) ion concentrations of 5–60 mg/L with a volume of 100 mL and pH 6 at room temperature.

The kinetics of the experiment used a solution of Fe(II), Fe(III), and Mn(II) with a concentration of 10 mg/L with a volume of 100 mL in a time range of 5–50 minutes, pH 6, and at room temperature, while thermodynamics was examined with temperature variations of 298, 308, 318, and 328°C. The number of ions adsorbed per gram (g) of the CaO/Fe₃O₄ composite was calculated using the following formula:

$$q_e = \frac{C_0 - C_t}{C_0} \quad (1)$$

where: C_0 and C_t – the initial and final concentrations of metal ions (mg/L).

The adsorption of total Fe and Mn ions from AMD was carried out with variations in the mass of the CaO/Fe₃O₄ composite in the range of 0.1–0.5 g, while the volume of acid mine drainage was 100 mL with a contact time of 60 minutes. The concentrations of Fe(total) and Mn(II) ions before and after the addition of the composite were measured using AAS. In addition, the change in pH of the solution was also determined with the addition of the CaO/Fe₃O₄ composite.

RESULTS AND DISCUSSION

Characterization of the CaO/Fe₃O₄ composite

The XRD spectra of CaO, Fe₃O₄, and the CaO/Fe₃O₄ composite are presented in Figure 1. In the CaO structure, several peaks were observed at 2θ , ie 32.51°, 36.97°, 54.01°, 64.23°, 67.01° according to the crystal phase (111), (200), (220), (311), and (222) (JCPDS No. 48-1467 standard CaO cards). Some of the peaks that appear at 17.89°, 28.61°, and 48.02° are attributed to Ca(OH)₂ according to (JCPDS No. 72-0156 standard cards). The presence of Ca(OH)₂ is due to the absorption of H₂O by CaO which is difficult to avoid. Moreover, the Fe₃O₄ had a characteristic peak intensity at 2θ namely 35.57° (311). The other peaks are 30.41°, 43.57°, 53.71°, 57.49°, and 62.93° indicating crystal planes (220), (400), (422), (511), and (440), respectively, which are inverse spinel crystal structure (JCPDS No. 89-0691 standard cards Fe₃O₄) [Reddy et al., 2018]. The composite peak of CaO/Fe₃O₄ showed a combined peak of CaO and Fe₃O₄ where the peak of Fe₃O₄ is lower than the pure form. Another study showed a similar pattern with activated carbon-Fe₃O₄ and hydroxyapatite-Fe₃O₄ composites [Duan et al., 2020;

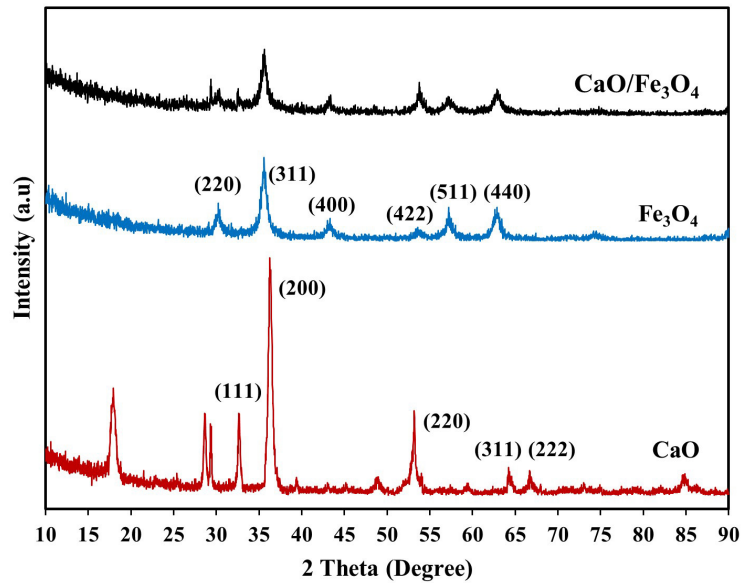


Figure 1. XRD patterns of CaO, Fe_3O_4 and $\text{CaO}/\text{Fe}_3\text{O}_4$ composite

Biedrzycka et al., 2021]. The average crystal size calculated using the Scherrer formula showed that CaO, Fe_3O_4 , and the $\text{CaO}/\text{Fe}_3\text{O}_4$ composites had crystal sizes of 9.39, 7.09, and 18.23 nm. This is in line with previous studies, where the crystal size of NiFe_2O_4 is lower than the activated carbon/ NiFe_2O_4 composites [Jiang et al., 2015].

Table 1 shows the specific surface area, pore volume, and average pore diameter of CaO, Fe_3O_4 , and the $\text{CaO}/\text{Fe}_3\text{O}_4$ composites. The source and method of CaO synthesis affect the value of the specific surface area. On the basis of the results, the specific surface area of CaO was $137.402 \text{ m}^2/\text{g}$, which is larger than Fe_3O_4 and the $\text{CaO}/\text{Fe}_3\text{O}_4$ composites. Some of the CaO pores were filled with nano-sized Fe_3O_4 ; hence, the specific surface area of the $\text{CaO}/\text{Fe}_3\text{O}_4$ composite was reduced. According to the definition of pore size by IUPAC, a material is classified as macropore, mesopore, and micropore when the size is $>50 \text{ nm}$, between $2\text{--}50 \text{ nm}$, and $< 2 \text{ nm}$, respectively. The average pore diameter for all samples

ranged from $2\text{--}50 \text{ nm}$. They were classified as mesopores. Furthermore, the specific surface area of the $\text{CaO}/\text{Fe}_3\text{O}_4$ composite was similar to CaO. These results indicate that CaO is the main component of the composite.

The morphology of CaO, Fe_3O_4 , and the $\text{CaO}/\text{Fe}_3\text{O}_4$ composite is presented in Figure 2. There is a change in the morphology of CaO before and after impregnation with Fe_3O_4 . The surface of the $\text{CaO}/\text{Fe}_3\text{O}_4$ composite is similar to CaO, indicating that CaO is the major component. The surface of Fe_3O_4 appeared as tiny particles culminating in a tendency to form agglomerations.

The SEM mapping of the $\text{CaO}/\text{Fe}_3\text{O}_4$ composite showed a heterogeneous surface shape, Fe (blue) appeared to be distributed on most of the CaO surfaces which were green (Ca) and red (O), as shown in Figure 3a. On the basis of the EDS analysis in Figure 3b, the $\text{CaO}/\text{Fe}_3\text{O}_4$ composite consists of 25.8, 44.3 and 28.6% Ca, O, and Fe, respectively, indicating that the composite has been successfully synthesized.

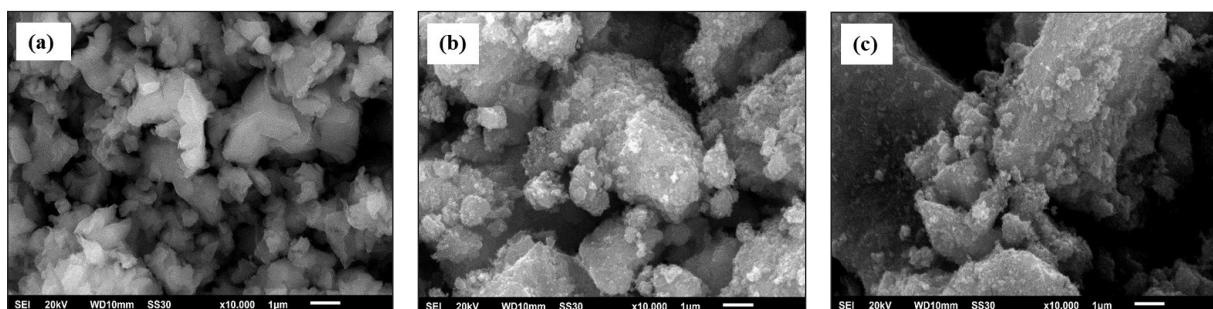


Figure 2. Morphology of (a) CaO, (b) Fe_3O_4 , and (c) $\text{CaO}/\text{Fe}_3\text{O}_4$ composite

Table 1. Specific surface area of CaO, Fe₃O₄ and the CaO/Fe₃O₄ composite

Compund	BET surface area (m ² /g)	Pore volume (cm ³ /g)	Average pore diameter (nm)
CaO	137.402	0.265	7.724
Fe ₃ O ₄	72.162	0.236	8.372
CaO/Fe ₃ O ₄ composite	110.546	0.252	7.868

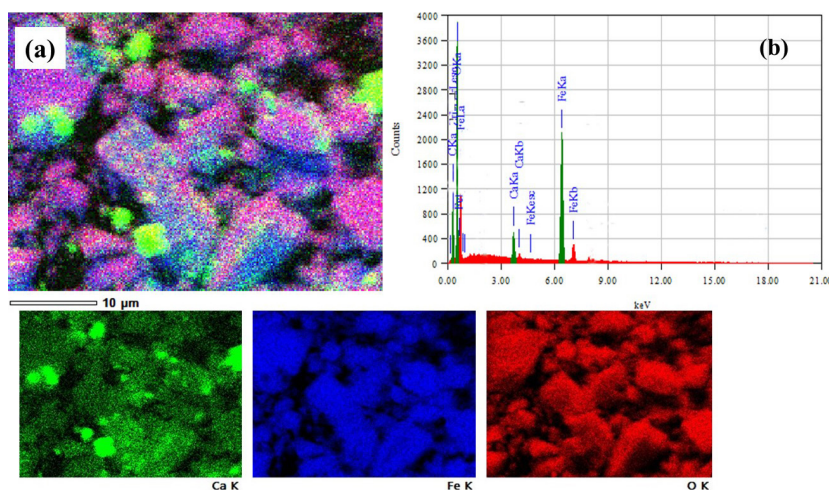


Figure 3. (a) SEM mapping and (b) EDS spectra of CaO/Fe₃O₄ composite

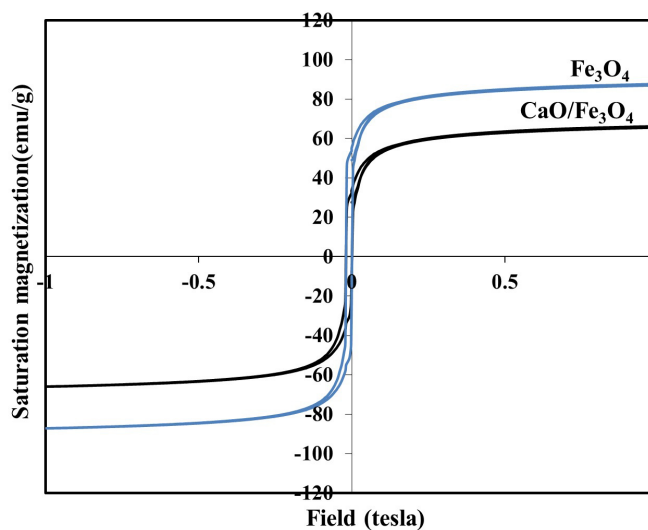


Figure 4. Saturation magnetization curves of Fe₃O₄ and the CaO/Fe₃O₄ composite

The magnetic properties of Fe₃O₄ and the CaO/Fe₃O₄ composite were investigated using VSM at room temperature, the hysteresis loops curve is presented in Figure 4. The saturation magnetization (Ms) of Ca/Fe₃O₄ composite was 65.49 emu/g, which is smaller than Fe₃O₄ at 86.84 emu/g. The Fe₃O₄ synthesized by means of the coprecipitation method was greater compared to another study that used the same method, namely 72 emu/g [Wu et al., 2021]. CaO is non-magnetic, its incorporation with Fe₃O₄ causes a decrease in magnetic properties. Meanwhile, the magnetic

properties of the CaO/Fe₃O₄ composite are excellent, and it can easily and quickly be separated from the solution using a magnet after the adsorption process.

Adsorption studies

Effect of pH, contact time, and initial concentration

The pH of the solution is an important parameter in adsorption efficiency, the effect was demonstrated in the range of 2–9. Figure 5a shows

that the adsorption capacity increases from pH 2 to 6, then followed by a decline at pH > 6, thereby decreasing the adsorption capacity. A similar trend was observed for the adsorption of Fe(II) and Mn(II) ions, but the adsorption capacity of Mn was smaller than Fe. The solubility of metal ions is greater at acidic pH conditions, but at acidic pH, there is competition between H⁺ ions and metal ions to be adsorbed on the CaO/Fe₃O₄ composite. At pH > 6, a reduction occurs in the adsorbed metal ions, this phenomenon is related to the reaction with hydroxides to form precipitates [Zhang et al., 2014]. When metal hydroxides are formed, they settle and fall to the bottom of the solution, or block the surface of the adsorbent [Shi et al., 2020]. On the basis of the results, 6 is the optimum pH in the adsorption process.

Contact time was shown to affect the adsorption process, Figure 5b shows that the longer the contact ranging from 0–60 minutes between metal ions and the CaO/Fe₃O₄ composite, the higher removal of metals ions. High adsorption in the early stages indicates that there are still several empty pores on the adsorbent and the occurrence

of a diffusion mechanism. This shows that the adsorption rate of Fe(II), Fe(III), and Mn(II) ions in the CaO/Fe₃O₄ composite is high. After 60 minutes, there was no significant change in the adsorption capacity, culminating in equilibrium and rearrangement [Chakraborty et al., 2021].

Figure 5c shows the effect of the initial concentration of metal ions on the adsorption capacity of the CaO/Fe₃O₄ composite. The greater the initial concentration, the greater the adsorption. Although the adsorption increased along with the metal ion concentration, there was a decrease in the percentage of adsorption. This might be due to the lack of available active sites required for the initial high concentration of metal ions [Zhang et al., 2014], a similar phenomenon was also reported in other studies [Chakraborty et al., 2021].

Adsorption kinetics

Adsorption kinetics is one of the important parameters to evaluate the properties of a good adsorbent, namely the rate of absorption. The adsorption process is controlled by several steps (i)

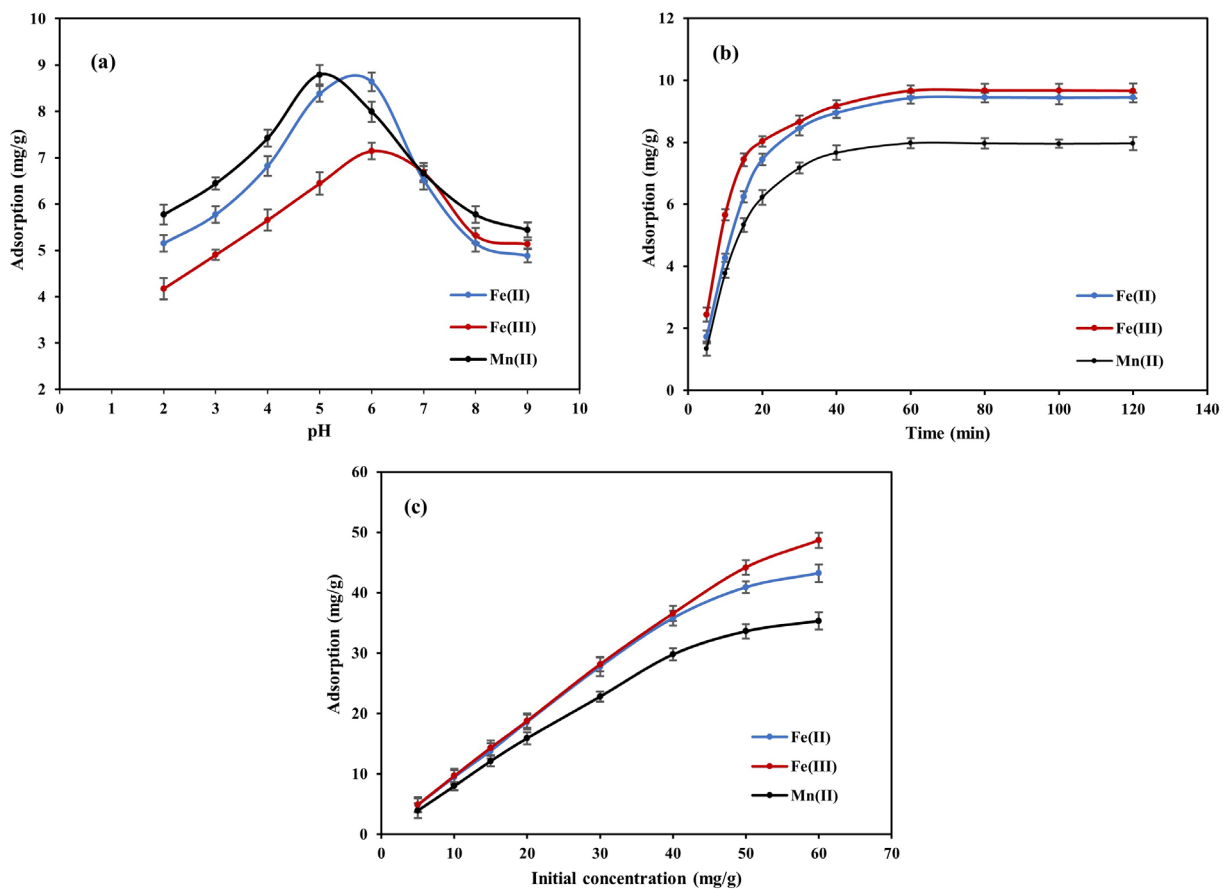


Figure 5. Effect of (a) pH, (b) contact time, and (c) initial concentration for adsorption of Fe(II), Fe(III) and Mn(II) ions onto CaO/Fe₃O₄ composite

transport of pollutants to the surface of the adsorbent, (ii) transfer of pollutants from the surface of the adsorbent to the active side of the intra-particle space, followed by rearrangement or maintenance in active sites, and (iii) formation of complex compounds or precipitation [Keshavarz et al., 2021]. Two commonly used adsorption kinetics models are pseudo-first-order and pseudo-second-order. The pseudo-first-order kinetic model assumes that the rate of adsorbed metal ions is proportional to the number of active sites on the adsorbent surface. The equation is as follows:

$$\ln (q_e - q_t) = \ln q_e - k_1 \cdot t \quad (2)$$

where: q_e and q_t – the number of metal ions adsorbed at equilibrium and t (time), k_1 (min^{-1}) is a pseudo-first-order constant. The pseudo-second-order equation is expressed in the equation:

$$\frac{t}{q_t} = \frac{1}{k_2 q_e^2} + \frac{t}{q_e} \quad (3)$$

where: q_e and q_t – the number of metal ions adsorbed (mg/g) at equilibrium and t (time), k_2 (g/mg min) is a pseudo-first-order constant.

Table 2 shows the pseudo-first-order and pseudo-second-order kinetic parameters. The pseudo-first-order is more suitable to describe the adsorption kinetics of Fe(II), Fe(III), and Mn(II) ions than the second-order with values in pseudo-first-order > pseudo-second-order. Meanwhile, the calculation value is greater than both pseudo-first-order and pseudo-second-order experiments. The pseudo-first-order adsorption kinetics of Fe(II), Fe(III), and Mn(II) ions using a CaO/Fe₃O₄ composite are presented in Figure 6.

Adsorption isotherm

The adsorption isotherm describes the overall process and how metal ions namely Fe and Mn interact with the CaO/Fe₃O₄ composite. It is important to identify the model that describes the distribution of the adsorbate on the adsorbent, the adsorption characteristics at equilibrium and predicts the mechanism [Langmuir, 1918]. This study used two models, namely the Langmuir and the Freundlich isotherms. The Langmuir model assumes that adsorption is a monolayer on

Table 2. Parameters of kinetic model for the adsorption of Fe(II), Fe(III), and Mn(II) ions onto the CaO/Fe₃O₄ composite

Kinetics models	Parameters	Fe(II)	Fe(III)	Mn(II)
Pseudo-first-order	R^2	0.995	0.994	0.999
	K_1 (min^{-1})	0.078	0.066	0.084
	$q_{e,calc}$ (mg/g)	10.451	10.780	9.320
Pseudo-second-order	R^2	0.912	0.970	0.959
	K_2 ($\text{g/mg}\cdot\text{min}$)	0.0030	0.0034	0.0044
	$q_{e,calc}$ (mg/g)	14.392	14.710	11.351
	$q_{e,exp}$ (mg/g)	9.491	9.670	7.672

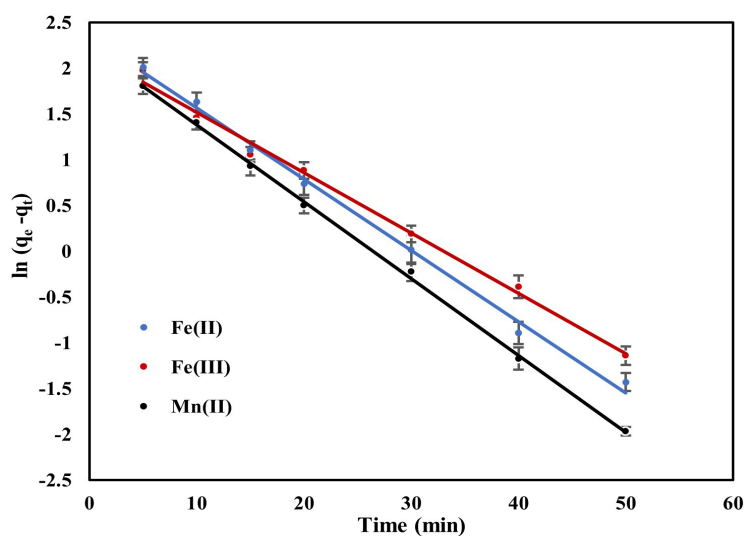


Figure 6. The pseudo-first-order kinetic model for adsorption of Fe(II), Fe(III), and Mn(II) ions onto the CaO/Fe₃O₄ composite

a homogeneous surface with no interaction. The equation that describes this isotherm is as follows:

$$\frac{C_e}{q_e} = \frac{C_e}{q_m} + \frac{1}{K_L q_m} \quad (4)$$

where: C_e – the concentration of metal ions at equilibrium (mg/L), q_e – the number of metal ions adsorbed at equilibrium (mg/g), q_m – the maximum adsorption capacity (mg/g), K_L – the Langmuir constant (L/mg).

Meanwhile, Freundlich's isotherm model assumes that the adsorbent surface is heterogeneous and the active site surface has different energies [Freundlich, 1906]. The equation is expressed as follows:

$$q_e = K_F C_e^{1/n} \quad (5)$$

The equation can also be expressed in the form:

$$\log q_e = \log K_F + \frac{1}{n} \log C_e \quad (6)$$

where: K_L – Freundlich's constant, $1/n$ – indicates the adsorption intensity.

Table 3 presents the Langmuir and Freundlich isotherm model parameters on the adsorption of Fe(II), Fe(III), and Mn(II) ions using the CaO/Fe₃O₄ composite. The Langmuir isotherm showed a higher correlation coefficient (R^2) than Freundlich, indicating greater suitability for the adsorption equilibrium data. The adsorption capacity (q_m) of the CaO/Fe₃O₄ composite to Fe(III) ions was 75.758 mg/g, which is greater than Fe(II) and Mn(II) ions as much as 67.567 and 53.192 mg/g. The adsorption capacity of Fe(III) ions > Fe(II) ions similar to the results obtained using polyaniline-coated sawdust [Mansoor and Abbasitabar, 2020] and thiourea cross-linked chitosan [Dai et al., 2012]. Besides, the adsorption capacity of Fe(II) > Mn(II) ions similar with the result obtained from rice husk ash [Zhang et al., 2014] and activated carbon from sawdust [El Sherif et al., 2013]. Figure 7 presents the Langmuir isotherm model in the adsorption of Fe(II), Fe(III), and Mn(II) ions.

Table 4 shows the comparison of the adsorption capacity of several adsorbents to Fe(II),

Table 3. Parameters of the Langmuir and Freundlich isotherm models for the adsorption of Fe(II), Fe(III), and Mn(II) ions onto the CaCO₃/Fe₃O₄ composite

Isotherm models	Parameters	Fe(II)	Fe(III)	Mn(II)
Langmuir	R^2	0.991	0.998	0.992
	K_L	0.297	0.429	0.102
	q_m	67.567	75.758	53.192
Freundlich	R^2	0.985	0.952	0.941
	K_F	13.701	16.370	4.921
	n	1.557	2.118	1.415

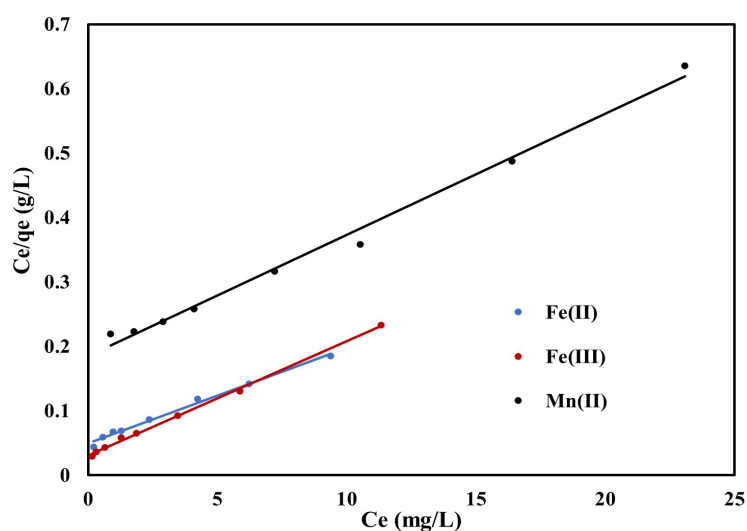


Figure 7. Langmuir isotherm plots for the adsorption of Fe(II), Fe(III), and Mn(II) ions in the CaO/Fe₃O₄ composite

Table 4. The adsorption capacity of Fe(II), Fe(III), and Mn(II) ions onto some adsorbent

Ions	Adsorbents	Contact time (min)	pH	Adsorption capacity (mg/g)	References
Fe (II)	Polyaniline Coated Sawdust	10	4	35.29	[Mansoor et al., 2020]
	Thiourea Cross-Linked Chitosan	60	5	48.30	[Dai et al., 2012]
	Activated carbon from sawdust	30	7	6.54	[El-Sherif et al., 2013]
	Pomegranate peel (carbon active)	40	6	18.52	[Moghadam et al., 2013]
	SiO ₂ from rice husk ash	20	5	9.0	[Nguyen et al., 2019]
	CaCO ₃ /Fe ₃ O ₄ composite	60	6	67.567	In this study
Fe(III)	Hazenut hull	60	3	13.59	[Sheilbani et al., 2012]
	Thiourea Cross-Linked Chitosan	60	5	71.90	[Dai et al., 2012]
	Orange peel	100	3.5	18.1992	[Lugo-lugo et al., 2012]
	Brown bentonite	120	-	16.86	[Baklar et al., 2020]
	Polyaniline Coated Sawdust	10	4	40.65	[Mansoor et al., 2020]
	CaCO ₃ /Fe ₃ O ₄ composite	60	6	75.758	In this study
Mn(II)	Risk hush ash	60	6	3.02	[Zhang et al., 2014]
	Activated carbon from bombax malabaricum	50	7	8.2	[Emmanuel and Rao, 2009]
	Chitosan/polyethylene glycol	80	5	21.7	[Reiad et al., 2012]
	Activated carbon from sawdust	30	8	4.72	[El-Sherif et al., 2013]
	Manganese Oxide-Coated Hollow Polymethylmethacrylate	70	7	8.374	[Dutta et al., 2021]
	CaCO ₃ /Fe ₃ O ₄ composite	60	6	53.192	In this study

Fe(III), and Mn(II) ions. The adsorption capacity has varying values for different adsorbents depending on the physical and chemical properties of the adsorbent used. The CaO/Fe₃O₄ composite in this study has a better adsorption capacity than other adsorbents.

Adsorption thermodynamic

Adsorption thermodynamics was determined to confirm the feasibility and spontaneity of the metal ion adsorption process [Fororoutan et al., 2021]. The thermodynamic parameters include standard Gibbs free energy (ΔG°), enthalpy (ΔH°), and entropy (ΔS°). The Gibbs free energy is expressed in the equation:

$$\Delta G^\circ = -RT \ln K_C \quad (7)$$

$$\ln K_C = \frac{\Delta S^\circ}{R} - \frac{\Delta H^\circ}{RT} \quad (8)$$

where: R – the universal gas constant ($8.314 \cdot 10^{-3}$ kJ/mol·K), T – the temperature (K), K_C – the equilibrium constant.

To determine the values of ΔH° and ΔS° based on the slope and intercept of the plot $\ln K_C$ Versus $1/T$. The adsorption thermodynamics evaluation was carried out at temperatures of 298, 308, 318, and 328 K, as presented in Table 5. The calculated

ΔG° value is negative, indicating that the adsorption process runs spontaneously, but it also implies that the reaction is favorable at a high temperature [Subbaiah and Kim, 2016]. A negative ΔH° value indicates that the interaction between metal ions is exothermic.

FTIR characterization before and after adsorption

The FTIR spectra of the CaO and CaO/Fe₃O₄ composites before and after the adsorption process in the range of 400–4000 cm⁻¹ are presented in Figure 8. The wavenumber around 3400 cm⁻¹ for CaO and CaO/Fe₃O₄ composites is a characteristic of O-H stretching vibration potentially from water absorption. In CaO, there was a strong peak at 3641.6 cm⁻¹ which correlates with the presence of a hydroxyl group stretching peak of hydroxide [Jitjamnong et al., 2019], structural OH groups of Ca(OH)₂ [Mar and Somsook, 2012], and the presence of Ca(OH)₂ on the adsorbent surface. The peaks at 1425.3 and 871.8 cm⁻¹ are plane vibration groups of carbonates (C-O bonds). This peak appears in CaO and the CaO/Fe₃O₄ composites with different intensities indicating the presence of calcium carbonate in the adsorbent. Generally, this peak appears at CaO from natural shell

Table 5. Parameter for adsorption thermodynamic of Fe(II), Fe(III), and Mn(II) ions onto the CaCO₃/Fe₃O₄ composite

Ions	Parameters	Temperature (K)			
		298	308	318	328
Fe(II)	ΔG° (KJ/mol)	-10.537	-10.753	-10.969	-11.186
	ΔH° (KJ/mol)	-4.098			
	ΔS° (KJ/mol)	0.022			
Fe(III)	ΔG° (KJ/mol)	-14.094	-14.391	-14.688	-14.986
	ΔH° (KJ/mol)	-5.235			
	ΔS° (KJ/mol)	0.029			
Mn(II)	ΔG° (KJ/mol)	-7.297	-7.435	-7.572	-7.709
	ΔH° (KJ/mol)	-3.202			
	ΔS° (KJ/mol)	0.014			

[Jitjamnong et al., 2019]. The wavenumber at 416.6 cm⁻¹ suggests the peak of the Ca-O bond. This result is similar to CaO synthesized from eggshell, appearing at a wavenumber of 412.0 cm⁻¹ [Hossain et al., 2021].

The wavenumber that indicates the presence of Fe-O bonds in the CaO/Fe₃O₄ composite appeared at 541.9 cm⁻¹. After the adsorption process, the same peak still appeared at adjacent wavenumbers, namely 542.8 and 541.6 cm⁻¹ but with different intensities. Another study reported that the Mn-O bonds detected at wavenumbers 462, 520, and 702 cm⁻¹ are due to its vibrations [Stella et al., 2014]. On the basis of the results, the CaO/Fe₃O₄ composite after adsorption of Mn(II) ion had peaks at wavenumbers 449.4, 545.7, and 709.4 cm⁻¹. After the adsorption process, there was an overlapping bond between Fe-O from

Fe₃O₄ as well as the adsorbed Fe(II), Fe(III), and Mn(II) ions. The shift in wavenumber < 10 cm⁻¹ and changes in intensity indicate that the adsorption process is between metal ions and the CaO/Fe₃O₄ composites [Kasirajan et al., 2022].

Treatment of acid mine drainage by the CaO/Fe₃O₄ composite

In reality, AMD consists of several other types of metal ions apart from Fe and Mn such as As, Cu, Pb, and Zn [Carrilo-Gonzalez et al., 2022; Motsi et al., 2011]. This study focused on 2 types of metal ions, namely Fe and Mn, according to the quality standards of AMD in Indonesia. Fe ions in AMD consist of Fe(II) and Fe(III). The formation of Fe(III) from the oxidation of pyrite compounds is as follows [Nordstrom et al., 2015; Choi et al., 2007]:

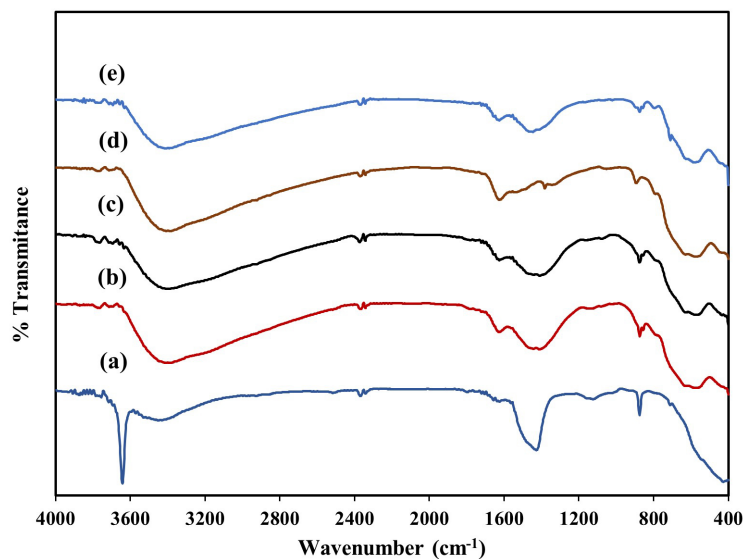
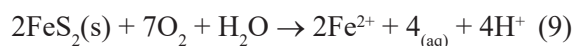


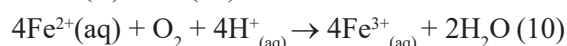
Figure 8. Spectra FTIR of (a) CaO, (b) CaO/Fe₃O₄ composite, CaO/Fe₃O₄ composite after the adsorption of (c) Fe(II), (d) Fe(III), and (e) Mn(II) ions

Table 6. Characteristic of AMD before and after treatment using the CaO/Fe₃O₄ composite

Parameters	Before treatment	After treatment using CaO/Fe ₃ O ₄ composite (g)					Quality standards
		0.1	0.2	0.3	0.4	0.5	
Fe (mg/L)	45.68	38.36	20.56	12.54	4.38	4.42	Max 7
Mn (mg/L)	8.74	7.72	3.34	0.86	0.21	0.20	Max 4
pH	3.8	4.8	5.6	6.2	6.9	7.0	6-9



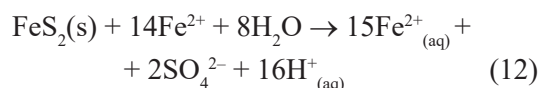
Furthermore, there is an oxidation reaction from Fe(II) to Fe(III)



Fe(III) undergoes hydrolysis



There is a combination reaction of pyrite with Fe(II) ions



In general, the reaction can be written as:

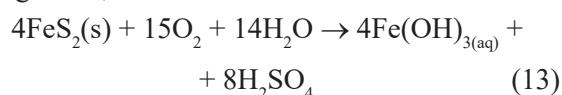


Table 6 shows the ion content of Fe, Mn, and pH of AMD before and after treatment using the CaO/Fe₃O₄ composite. According to the Indonesian Ministry of Environment No. 113 (2003), the quality standard of AMD, the maximum concentration of Fe and Mn, is 7 and 4 mg/L, while the pH is 6–9. On the basis of the results, the Fe and Mn ions concentration and the pH in AMD are above the quality standard. The AMD treatment was carried out at a volume of 100 mL with mass of the CaO/Fe₃O₄ composite 0.1, 0.2, 0.3, 0.4, and 0.5 g, and a contact time of 60 minutes. The results showed that the greater the addition of the composite, the higher the Fe and Mn ions adsorbed, along with increased pH. With the addition of 0.1 g composite to AMD, only some Fe and Mn ions were adsorbed, due to the competition between the metal ions. Apart from Fe and Mn ions, other metal ions are also adsorbed. A previous study showed that the adsorption capacity of organic biomixture to some metal ions from acid mine drainage is in the order of Fe > Zn > Cu > Mn [Raiman et al., 2021]. The type and adsorbent dose determine the amount of metal ions reduced [Carrilo-Gonzales et al., 2022]. The percentage reduction of Fe and Mn metal ions with the addition of 0.4 g CaO/Fe₃O₄ composite was

90.41% and 97.59%, respectively. Aside from a decrease in the concentration of metal ions, the addition of the composite also increased the pH of the solution. The concentration of Fe and Mn ions obtained from the treatment using CaO/Fe₃O₄ composites meets the AMD quality standards, while the pH increased from 3.8 to 6.9.

CONCLUSIONS

This study successfully modified CaO from green mussel shells with Fe₃O₄ to form a CaO/Fe₃O₄ magnetic composite. The saturation magnetization of the CaO/Fe₃O₄ composite was obtained at 65.49 emu/g. Furthermore, the experiment showed that the Langmuir isotherm model is more suitable for describing the adsorption mechanism of Fe(II), Fe(III), and Mn(II) ions using the CaO/Fe₃O₄ composite. The equilibrium data indicates that the adsorption of the metal ions was in the Pseudo-first-order, while the mean free energy suggests that the adsorption process occurred spontaneously. The CaO/Fe₃O₄ composite absorbed 90.41% Fe and 97.59% Fe ions, with an increase in pH from 3.8 to 6.9 from AMD. Therefore, the composite has the potential to be used for reducing pollution in AMD, specifically heavy metal ions.

Acknowledgments

The author is grateful to the Ministry of Education, Culture, Research, and Technology, Indonesia for funding the 2022 “Doctoral Dissertation Research Grant” scheme with contract number 0145.08/UN9.3.1/PL/2022.

REFERENCES

- Ahmaruzzaman M. 2011. Industrial wastes as low-cost potential adsorbents for the treatment of wastewater laden with heavy metals. *Advances in Colloid and Interface Science*, 166(1-2), 36–59.

2. Aprianti T., Afrah B.D., Agustina T.E. 2017. Acid Mine Drainage Treatment Using Activated Carbon Ceramic Adsorbent in Adsorption Column. *International Journal on Advanced Science Engineering Information Technology*, 7(4), 1241–1247.
3. Bakalar T., Kanuchova M., Girova A., Pavolova H., Hromada R., Hajduova Z. 2020. Characterization of Fe(III) adsorption onto zeolite and bentonite. *International Journal of Environmental Research and Public Health*, 17(16), 1–13.
4. Biedrzycka A., Skwarek E., Hanna U.M. 2021. Hydroxyapatite with magnetic core: synthesis methods, properties, adsorption and medical applications. *Advances in Colloid and Interface Science*, 291, 1–21.
5. Candeias C., Avila P.F., Silva E.F., Ferreira A., Salgueiro A.R., Teixeira J.P. 2014. Acid mine drainage from the Panasqueira mine and its influence on zezere river (Central Portugal). *Journal of African Earth Sciences*, 99(2), 705–712.
6. Carrilo-Gonzalez R., Garcia B.G.G., Gonzalez-Chavez M.D.C., Dominguez, F.A.S. 2022. Trace elements adsorption from solutions and acid mine drainage using agricultural by-products. *Soil and Sediment Contamination: An International Journal*, 31(3), 348–366.
7. Cazetta A.L., Pezoti O., Bedin K.C., Silva T.L. 2016. Magnetic activated carbon derived from biomass waste by concurrent synthesis: efficient adsorbent for toxic dyes. *ACS Sustainable Chemistry & Engineering*, 4(3), 1058–1068.
8. Chakraborty S., Mukherjee A., Das S., Maddela, N. R., Iram, S., Das, P. 2021. Study on isotherm, kinetics, thermodynamics of adsorption of crystal violet dye by calcium oxide modified fly ash. *Environmental Engineering Research*, 26(1), 1–9.
9. Chartrand M.M.G., Bunce N.J. 2003. Electrochemical remediation of acid mine drainage. *Journal of Applied Electrochemistry*, 33, 259–264.
10. Choi B.J., Lee S.M., Lee S.H. 2000. Coagulation treatment of landfill leachate using acid mine drainage (AMD). *Journal of Environmental Health Sciences*, 26(4), 129–133.
11. Choi J., Kwon D., Yang J., Lee J.Y., Park Y. 2007. Comparison of Fe and Mn removal using treatment agents for acid mine drainage. *Environmental Technology*, 30(5), 445–454.
12. Dai J., Ren F., Tao C.Y. 2012. Adsorption behavior of Fe(II) and Fe(III) ion on thiourea cross-linked chitosan with Fe(III) as template. *Molecule*, 17, 4388–4399.
13. Duan Z., Zhang W., Lu M., Shao Z., Huang W., Li J., Li Y., Mo J., Li Y., Chen C. 2020. Magnetic Fe₃O₄/activated carbon for combined adsorption and Fenton oxidation of 4-chlorophenol. *Carbon*, 167, 351–367.
14. Dutta D., Borah J.P., Puzari, A. 2021. Adsorption of Mn²⁺ from aqueous solution using manganese oxide-coated hollow polymethylmethacrylate. *Adsorption Science & Technology*, 2021, 1–10.
15. El-Sherif I.Y., Fathy N.A., Hanna, A.A. 2013. Removal of Mn(II) and Fe(II) ions from aqueous solution using precipitation and adsorption methods. *Journal of Applied Science Research*, 9(1), 233–239.
16. Emmanuel K.A., Rao A.V. 2009. Comparative study adsorption of Mn(II) from aqueous solutions on various activated carbon. *Journal of Chemistry*, 6(3), 693–704.
17. Foroutan R., Peighambaroust S.J., Mohammadi R., Omidvar M., Sorial G.A., Ramavandi B. 2020. Influence of chitosan and magnetic iron nanoparticles on chromium adsorption behavior of natural clay: Adaptive neuro-fuzzy inference modeling. *International Journal of Biological Macromolecules*, 151, 355–365.
18. Fororoutan R., Peighambaroust S.J., Ahmadi A., Akbari A., Farjadfar S., Ramavandi B. 2021. Adsorption mercury, cobalt, and nickel with a reclaimable and magnetic composite of hydroxyapatite/Fe₃O₄/polydopamine. *Journal of Environmental Chemical Engineering*, 9(4), 1–11.
19. Freundlich H. 1906. Über die adsorption in losungen. *Zeitschrift für Physikalische Chemie*, 57, 385–470.
20. Granados-Pichardo A., Granados-Correa F., Sanchez-Mendieta V., Hernadez-Mendoza H. 2020. New CaO-based adsorbents prepared by solution combustion and high-energy ball-milling processes for CO₂ adsorption: textural and structural influences. *Arabian Journal of Chemistry*, 13(1), 171–183.
21. Hossain M., Muntaha N., Goni L.K.M.O., Jamal M.S., Gafur M.A., Islam D., Fakhuruddin A.N.M. 2021. Triglyceride conversion of waste frying oil up to 98.46% using low concentration K⁺/CaO catalysts derived from eggshells. *ACS Omega*, 6(51), 35679–35691.
22. Jiang T., Liang Y., He Y, Wang Q. 2015. Activated carbon/NiFe₂O₄ magnetic composite: a magnetic adsorbent for the adsorption of methyl orange. *Journal of Environmental Chemical Engineering*, 3(3), 1740–1751.
23. Jitjamnong J., Luengnaruemitchai A., Samanwonga N., Chuaykarn N. 2019. Biodiesel production from canola oil and methanol using Ba impregnated calcium oxide with microwave irradiation assistance. *Chiang Mai Journal of Science*, 46(5), 987–1000.
24. Johnson D.B., Hallberg K.B. 2005. Acid mine drainage remediation options: a review. *Science of The Total Environment*, 338(1-2), 3–14.
25. Kasirajan R., Bekele A., Girma E. 2022. Adsorption of lead (Pb-II) using CaO-NPs synthesized by sol gel process from hen eggshell: response surface methodology for modeling, optimization and kinetics study. *South African Journal of Chemical Engineering*, 40, 209–229.

26. Kefeni, K.K., Msagati, T.A.M, Mamba B.B. 2017. Acid mine drainage: prevention, treatment options, and resource recovery: a review. *Journal of Cleaner Production*, 151, 475–493.
27. Keshavarz M., Foroutan R., Papari F., Bulgariu L., Esmaili H. 2021. Synthesis of CaO/Fe₂O₃ nanocomposite as an efficient nano adsorbent for the treatment of wastewater containing Cr (III). *Separation Science and Technology*, 56(8), 1328–1341.
28. Langmuir I. 1918. The adsorption of gases on plane surfaces of glass, mica and platinum. *Journal of the American Chemical Society*, 40(9), 1361-1403.
29. Li X., Guo Y., Cai J., Bao W. 2022. Experiment study on the treatment of acid mine drainage containing heavy metals with domestic waste pyrolysis ash. *Water Science & Technology*, 85(1), 3225–3238.
30. Liu L., Liu J., Zhao L., Yang Z., Lv C., Xue J., Tang A. 2019. Synthesis and characterization of magnetic Fe₃O₄@CaSiO₃ composites and evaluation of their adsorption characteristics for heavy metal ions. *Environmental Science and Pollution Research*, 26, 8721–8736.
31. Lugo-lugo V., Barrera-Diaz C., Urena-Nunex F., Bilyeu B., Linares-Hernandez I. 2012. Biosorption of Cr(III) and Fe(III) in single and binary system onto the pretreated orange peel. *Journal of Environmental Management*, 112, 120–127.
32. Mansoor S.J., Abbasitabar F. 2020. Adsorption Behavior of Fe(II) and Fe(III) ions on polyaniline coated sawdust: batch and fixed-bed studies. *Acta Chimica Slovenica*, 67, 36–46.
33. Mar W.W., Somsook E. 2012. Mathanolysis of soybean oil over KCl/CaO solid base catalyst for biodiesel production. *Science Asia*, 38, 90–94.
34. Markovic R., Bessho M., Masuda N., Stevanovic Z., Bozic D., Trujic T.A., Gardic V. 2020. New Approach of Metals Removal from Acid Mine Drainage. *Applied Science*, 10, 1–16.
35. Marxen J.C., Becker W., Finke, D, Hasse B., Epple M. 2003. Early mineralization in *Biomphalaria glabrata*: Microscopic and structural results. *Journal of Molluscan Studies*, 69, 113–121.
36. Mohan D., Chander S. 2006. Removal and recovery of metal ions from acid mine drainage using lignite—a low cost sorbent. *Journal of Hazardous Materials*, B137, 1545–1553.
37. Moghadam M.R., Nasirizadeh N., Dashti Z., Babanezhad E. 2013. Removal of Fe(II) from aqueous solution using pomegranate peel carbon: equilibrium and kinetic studies. *International Journal of Industrial Chemistry*, 4(19), 1–6.
38. Motsi T., Rowson N.A., Simmons M.J.H. 2011. Kinetic studies of the removal of heavy metals from acid mine drainage by natural zeolite. *International Journal of Mineral Processing*, 101(1–4), 42–49.
39. Nguyen T.T., Ma H.T., Avti P., Bashir M.J.K., Ng C.A., Wong L.Y., Jun H.K., Ngo Q.M., Tran N.Q. 2019. Adsorptive removal of iron using SiO₂ nanoparticles extracted from rice husk ash. *Journal of Analytical Methods in Chemistry*, 2019, 1–8.
40. Nordstrom D.K., Blowes D.W., Ptacek C.J. 2015. Hydrogeochemistry and microbiology of mine drainage: an update. *Applied Geochemistry*, 57, 3–16.
41. Nunez-gomez D., Rodrigues C., Lapolli F.R., Lobo-Rocio M.A. 2019. Adsorption of heavy metals from coal acid mine drainage by shrimp shell waste: isotherm and continuous-flow study. *Journal of Environmental Chemical Engineering*, 7(1), 1–10.
42. Orescanin V., Kollar R., 2012. A combined CaO/electrochemical treatment of the acid mine drainage from the “Robule” lake. *Journal of Environmental Science and Health Part A*, 47, 1186–1191.
43. Pereira T.C.B., Santos K.B.D., Lautert-Dutra W., Teodoro L.S.T., Almeida V.O, Weiler J., Schneider I.A.H., Bogo M.R. 2020. Acid mine drainage (AMD) treatment by neutralization: evaluation of physical-chemical performance and ecotoxicological effects on zebrafish (*danio rerio*) development. *Chemosphere*, 253, 1–9.
44. Raiman M.L., Briceno G., Schalchli H., Bornhardt C., Diez M.C. 2021. Alternative treatment for metal ions removal from acid mine drainage using an organic biomixture as a low cost adsorbent. *Environmental Technology & Innovation*, 24, 1–11.
45. Reddy I.N., Sreedhar A., Reddy Ch.V., Shim J., Cho M., Kim D., Gwag J.S., Yoo K. 2018. Enhanced visible-light photocatalytic performance of Fe₃O₄ nanopyrramids for water splitting and dye degradation. *Journal of Solid State Electrochemistry*, 22, 3535–3546.
46. Reiad N.A., Salam O.E.A., Abadir E.F., Harraz F.A. 2012. Adsorptive removal of iron and manganese ions from aqueous solutions with microporous chitosan/polyethylene glycol blend membrane. *Journal of Environmental Sciences*, 24(8), 1425–1432.
47. Rodriguez C., Leiva E. 2020. Enhanced Heavy Metal Removal from Acid Mine Drainage Wastewater Using Double-Oxidized Multiwalled Carbon Nanotubes. *Molecules*, 25(1), 1–22.
48. Shi N., Xi B., Tiang F., Ma X., Li H., Feng J., Xiong, S. 2020. Boosting Na⁺ storage ability of bimetallic M_{ox}W_{1-x}Se₂ with expanded interlayers. *Chemistry of European Journal*, 26(43), 9580–9588.
49. Sicupira D.C., Silva T.T., Ladeira A.C.Q., Mansur, M.B. 2015. Adsorption of manganese from acid mine drainage effluents using bone char: continuous fixed bed column and batch desorption studies. *Brazilian Journal of Chemical Engineering*, 32(2), 577–584.
50. Sisca V., Deska A., Syukri, Zilfa, Jamarun N. 2021. Synthesis and characterization of CaO limestone

- from Linatau Buo supported by TiO_2 as a heterogeneous catalyst in the production of biodiesel. *Indonesian Journal of Chemistry*, 21(4), 979–989.
51. Sheilbani A., Shishehbor M.R., Alaei H. 2012. Removal of Fe(III) ions from aqueous solution by hazelnut hull as an adsorbent. *International Journal of Industrial Chemistry*, 3(4), 1–4.
52. Stella C., Soundararajan N., Ramachandran K. 2014. Structural, optical, dielectric, and magnetic properties of $\text{Mn}_{1-x}\text{Co}_x\text{O}_2$ nanowires. *Superlattices and Microstructures*, 71, 203–210.
53. Subbaiah M.V., Kim, D.S. 2016. Adsorption of methyl orange from aqueous solution by aminated pumpkin seed powder: kinetics, isotherms, and thermodynamic studies. *Ecotoxicology and Environmental Safety*, 128, 109–117.
54. Thakur S., Singh S., Pal B. 2021. Superior adsorption removal of dye and high catalytic activity for transesterification reaction displayed by crystalline CaO nanocubes extracted from mollusk shell. *Fuel Processing Technology*, 213, 1–9.
55. Tong L., Fan R., Yang S., Zhang Q., Pan, Y. 2022. A technology review on treatment of acid mine drainage with bentonite-steel slag composite. *SN Applied Sciences*, 4(10), 1–11.
56. Trumm D. 2010. Selection of active and passive treatment system for AMD-flow charts for new Zealand conditions. *New Zealand Journal of Geology and Geophysics*, 53(2-3), 195–210.
57. Westholm L.J. Repo E., Silanpaa M. 2014. Filter materials for metal removal from mine drainage—a review. *Environmental Science and Pollution Research*, 21, 9109–9128.
58. White M.M., Chejlava M., Fried B., Sherma J. 2007. The concentration of calcium carbonate in shells of freshwater snails. *American Malacological Bulletin*, 22, 139–142.
59. Wu K., Huang W., Hung W., Tsai C. 2021. Modified expanded graphite/ Fe_3O_4 composite as an adsorbent of methylene blue: adsorption kinetics and isotherm. *Material Science & Engineering, B*, 266, 1–8
60. Yew Y.P., Shameli K., Miyake M., Khairudin N.B.A. Mohamad S.E., Naiki T., Lee K.X. 2020. Green biosynthesis of superparamagnetic magnetite Fe_3O_4 nanoparticles and biomedical applications in targeted anticancer drug delivery system: A review. *Arabian Journal of Chemistry*, 13(1), 2287–2308.
61. Zhang Y., Zhao J., Jiang Z., Shan D, Lu Y. 2014. Biosorption of Fe(II) and Mn(II) ions from aqueous solution by rice husk ash. *Biomed Research International*, 2014, 1–11.
62. Zhong C.M., Xu Z.L., Fang X.H., Cheng L. 2007. Treatment of acid mine drainage (AMD) by ultra-low-pressure reverse osmosis and nanofiltration. *Environmental Engineering Science*, 24(9), 1297–1306.